Electronic Supplementary Material (ESI) for Materials Chemistry Frontiers.
This journal is © the Partner Organisations 2019

# Supporting Information

## Hierarchical CoFe-layered double hydroxide and g-$C_3N_4$ heterostructures with enhanced bifunctional photo/electrocatalytic activity towards overall water splitting

Muhammad Arif,[ab] Ghulam Yasin,[ac] Muhammad Shakeel[a], Muhammad Asim Mushtaq,[ab] Wen Ye,[b] Xiaoyu Fang[b], Shengfu Ji,[a*] and DongpengYan[ab*]

[a]State Key Laboratory of Chemical Resource Engineering, Beijing University of Chemical Technology, Beijing 100029, China.

[b]Key Laboratory of Theoretical and Computational Photochemistry, Ministry of Education, College of Chemistry, Beijing Normal University, Beijing 100875, China.

[c]BUCT-CWRU International Joint Laboratory, State Key Laboratory of Organic−Inorganic Composites, Center for Soft Matter Science and Engineering, College of Energy, Beijing University of Chemical Technology, Beijing, China.

**Corresponding authors:**

Dongpeng Yan

Email: yandongpeng001@163.com,

Shengfu Ji

Email:jisf@mail.buct.edu.cn

## Table of Contents

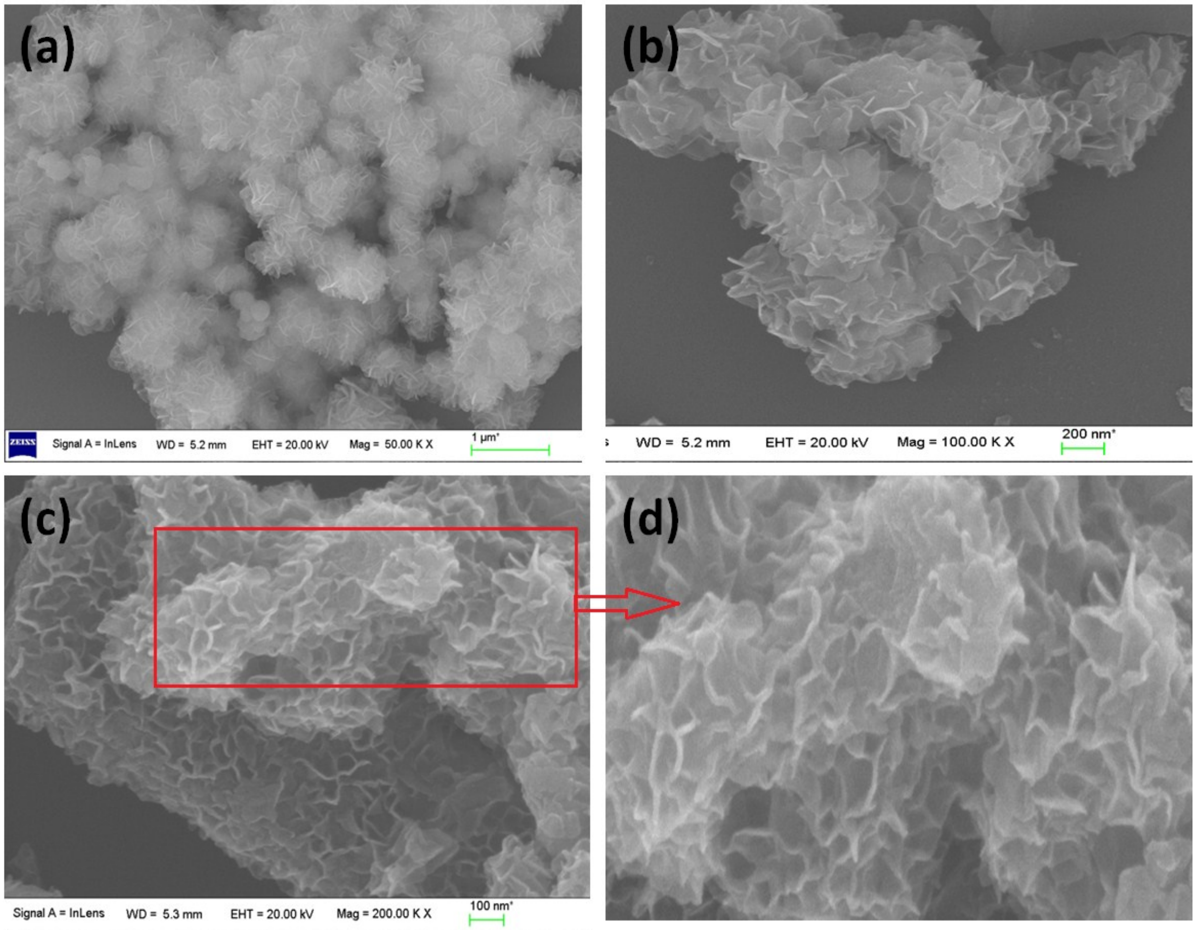


**Figure S1.** SEM images of CoFe-LDH (a and b) CoFe-LDH@g-$C_3N_4$ (10%) composite (c and d) at different resolutions

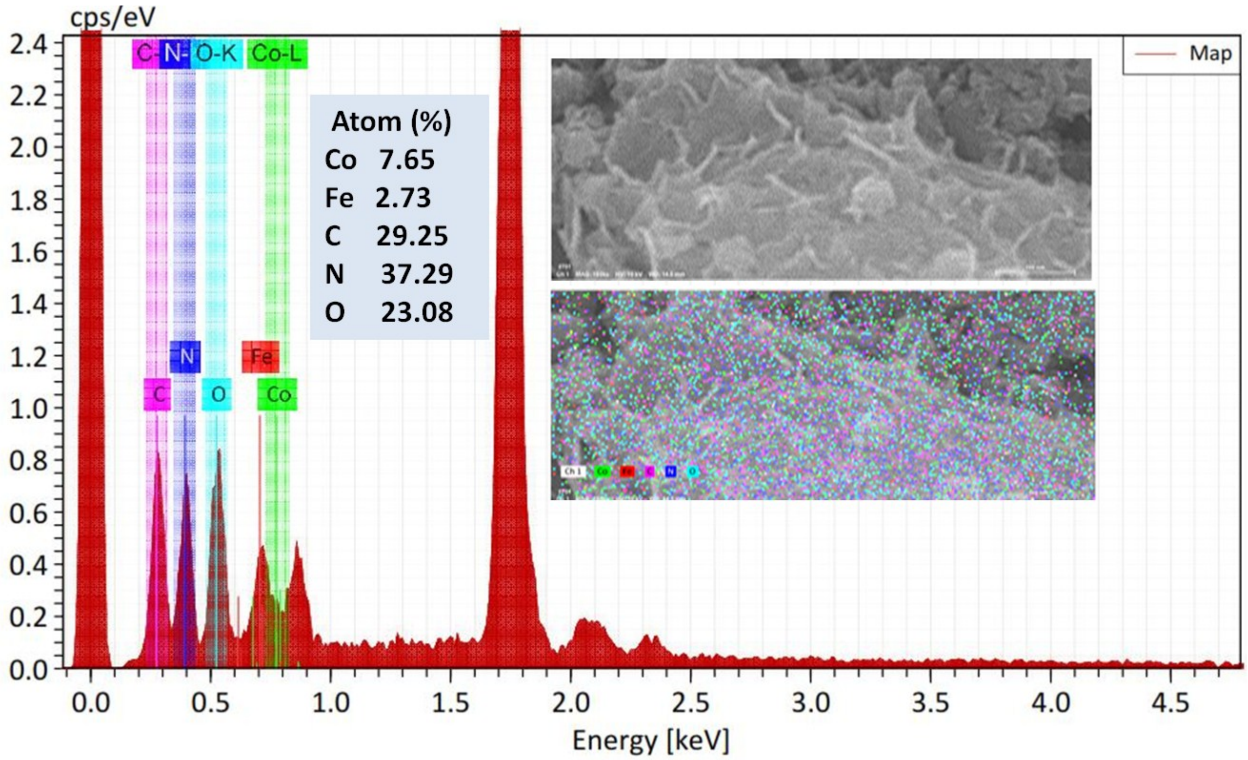


**Figure S2.** EDS spectrum of the CoFe-LDH@g-$C_3N_4$ (10%) composite

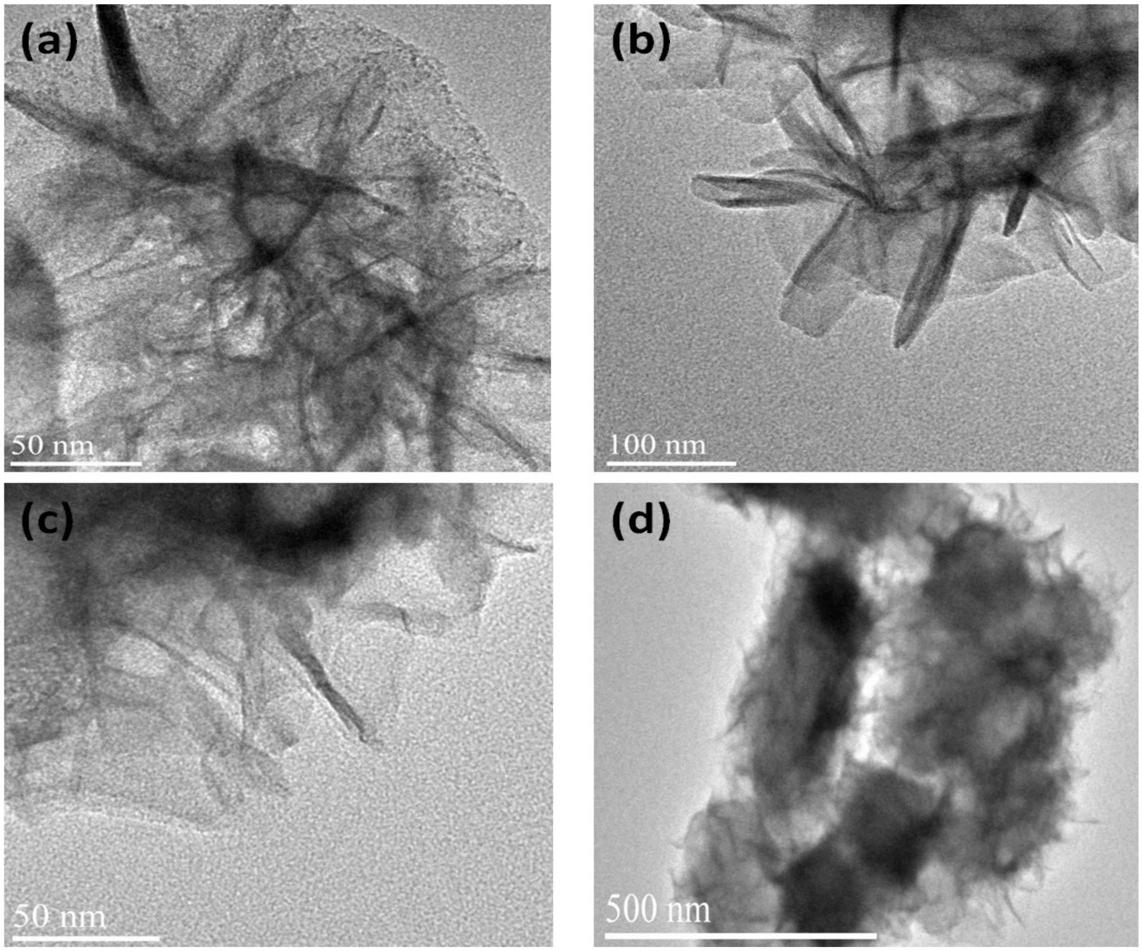


**Figure S3.** TEM images of CoFe-LDH (a and b) CoFe-LDH@g-$C_3N_4$ (10%) composite (c and d) at different resolutions

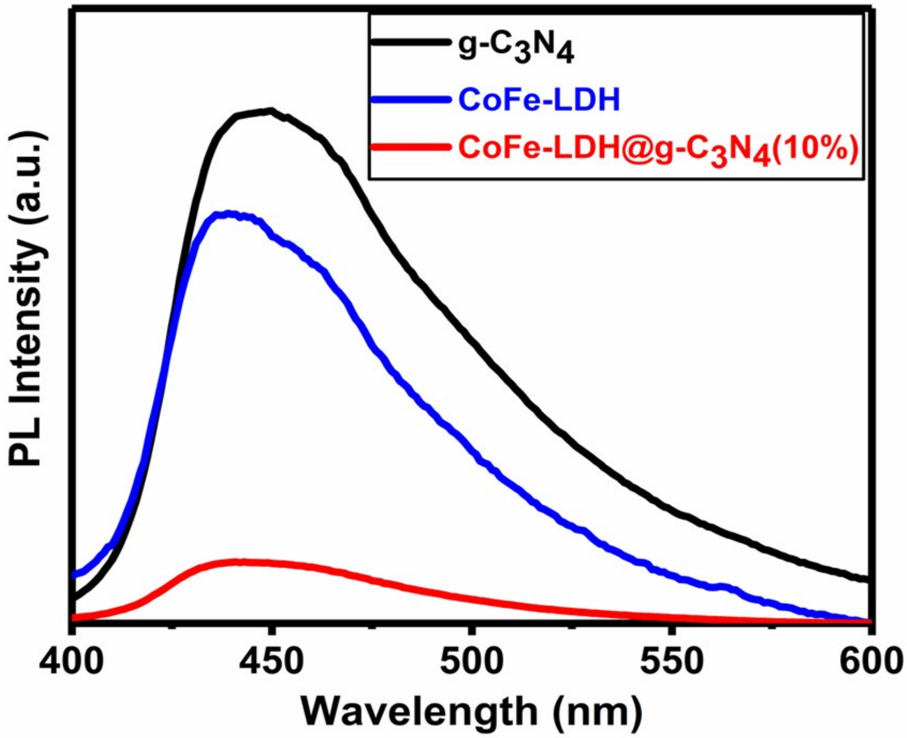


**Figure S4.** Photoluminescence spectra of g-$C_3N_4$, CoMn-LDH and CoMn-LDH@g-$C_3N_4$ (10%) composites

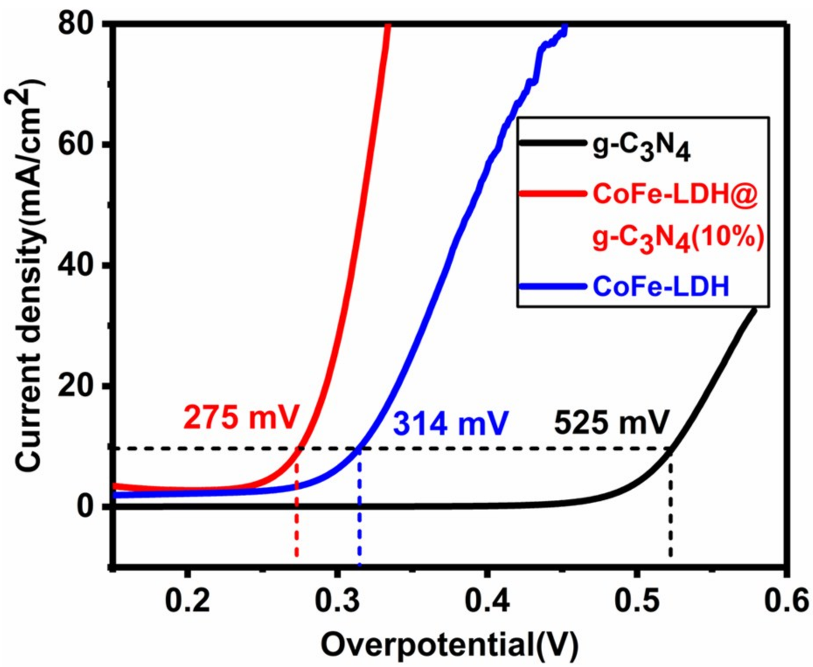


**Figure S5.** Linear scan voltammogram (LSV) OER curves of g-$C_3N_4$, CoFe-LDH and CoFe-LDH@g-$C_3N_4$ (10%)

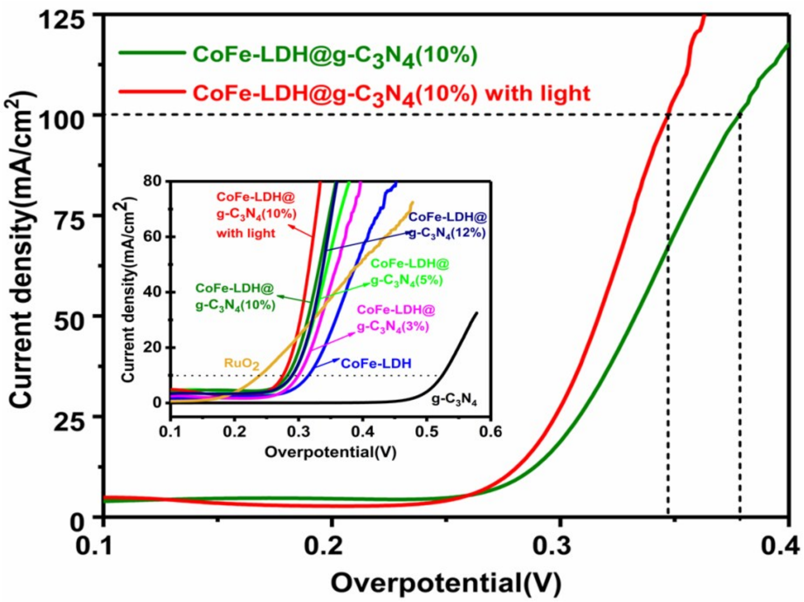


**Figure S6.** The comparison of the LSV curves for CoFe-LDH@g-$C_3N_4$ with and without light irradiations.

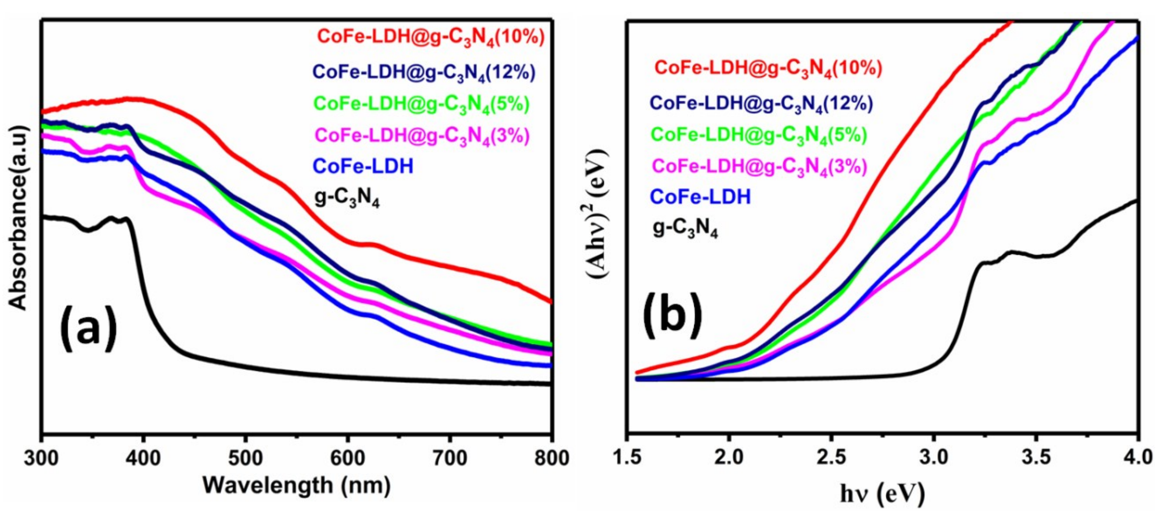


**Figure S7.** (a) UV–vis/DR spectroscopic analysis; (b) plots of $(\alpha h\nu)^2$ vs $(h\nu)$ for band gap energies of g-$C_3N_4$, CoFe-LDH and hierarchical CoFe-LDH@g-$C_3N_4$ heterostructures with different wt.% loading of g-$C_3N_4$.

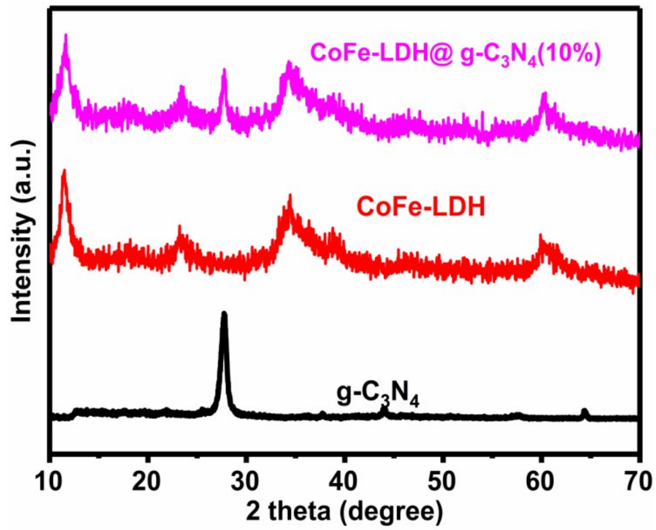


**Figure S8.** XRD patterns of g-$C_3N_4$, CoFe-LDH and CoFe-LDH@g-$C_3N_4$ composite materials.

The PXRD patterns of the as-synthesized g-$C_3N_4$, CoFe-LDH and CoFe-LDH@g-$C_3N_4$ composites are displayed in Figure S8. The diffraction patterns of pure and composite materials match well with the already reported in the literature.

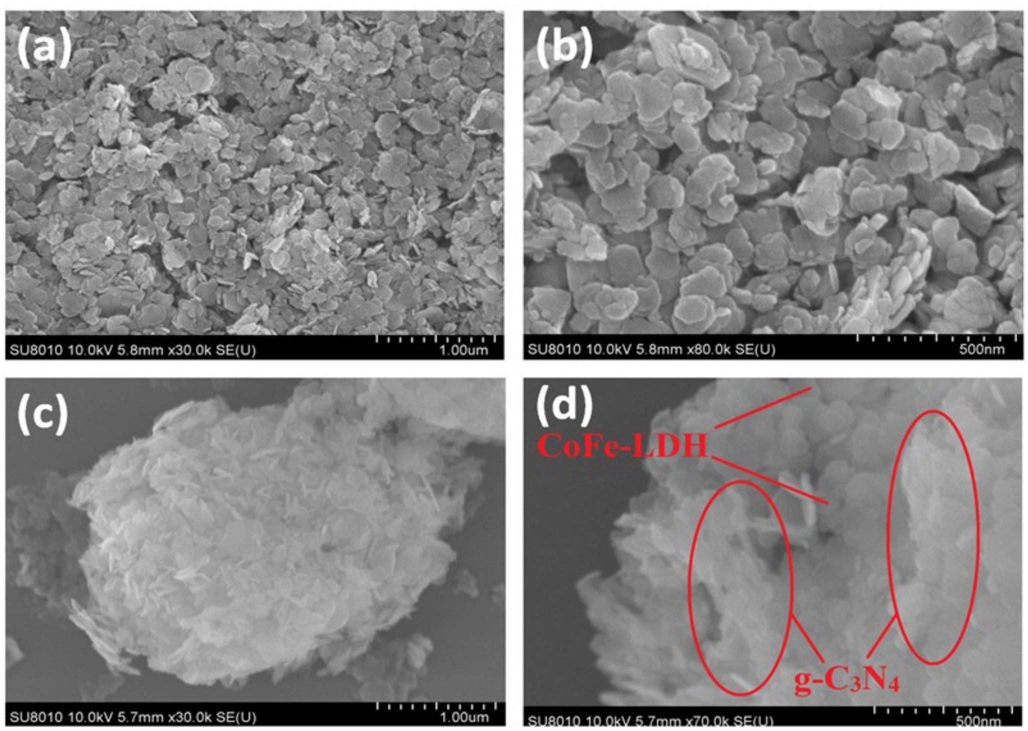


**Figure S9.** SEM images of CoFe-LDH (a and b) and CoFe-LDH@g-$C_3N_4$ composite (c and d).

The scanning electron microscope (SEM) was performed to analyze the morphological and structural features of the CoFe-LDH and CoFe-LDH@g-$C_3N_4$ prepared by coprecipitation and hydrothermal method. Typical SEM image of CoFe-LDH demonstrates 2D nanosheets-shaped structure (Figure S9). It Is observed that the morphology of CoFe-LDH and CoFe-LDH@g-$C_3N_4$ prepared by coprecipitation and hydrothermal method is totally different from solvothermal method.

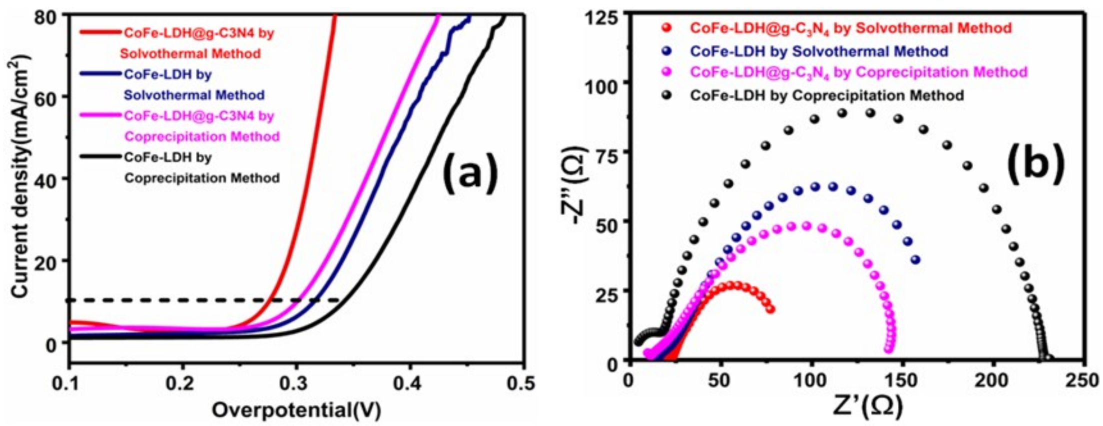


**Figure S10.** (a) Linear scan voltammogram (LSV) OER curves of CoFe-LDH and CoFe-LDH@ g-$C_3N_4$ with different methods, and (b) corresponding EIS spectra of CoFe-LDH and CoFe-LDH@g-$C_3N_4$ (10%).

The electrocatalytic activities of CoFe-LDH and CoFe-LDH@g-$C_3N_4$ composites (prepared by coprecipitation and hydrothermal method) were measured for both OER and electrochemical impedance spectroscopy (EIS) studies with a three electrode electrochemical cell system, as for hierarchical CoFe-LDH@g-$C_3N_4$ heterostructures. LSV OER curves for CoFe-LDH@g-$C_3N_4$ (10%) prepared by coprecipitation/hydrothermal method, and CoFe-LDH@g-$C_3N_4$ (10%) prepared by solvothermal method with light irradiation show overpotentials (potential to achieve a current density of 10 mA/cm$^2$) of 301 and 270 mV, respectively (Figure S10a). In our opinions, an efficient photo/electrochemical performance of composites prepared by solvothermal method is highly related to the hierarchical flower-like morphology, which has more exposed active sites and high surface area.

To further investigate the conductivity, EIS spectra of CoFe-LDH and CoFe-LDH@g-$C_3N_4$ composites prepared by different methods were performed in the three-electrode system as already discussed in detail in main manuscript. Various semi-circles in Nyquist plots at high frequency range can be correlated with $R_{ct}$ of the as-synthesized electrocatalysts. Therefore, EIS results confirm that the hierarchical CoFe-LDH@g-$C_3N_4$ shows a much lower $R_{ct}$ (76 Ω) relative to CoFe-LDH@g-$C_3N_4$ prepared by coprecipitation and hydrothermal method $R_{ct}$ (143 Ω), symbol of its effective electron-transfer behavior during the electrochemical reaction (Figure S10b). Excellent photoelectrocatalytic activities of CoFe-LDH@g-$C_3N_4$ are attributed to flower-like hierarchical structure, in which the high surface area and more exposed active sites could contribute to the enhancement of light harvesting capability, and facilitate the charge transportation within the heterostructure.

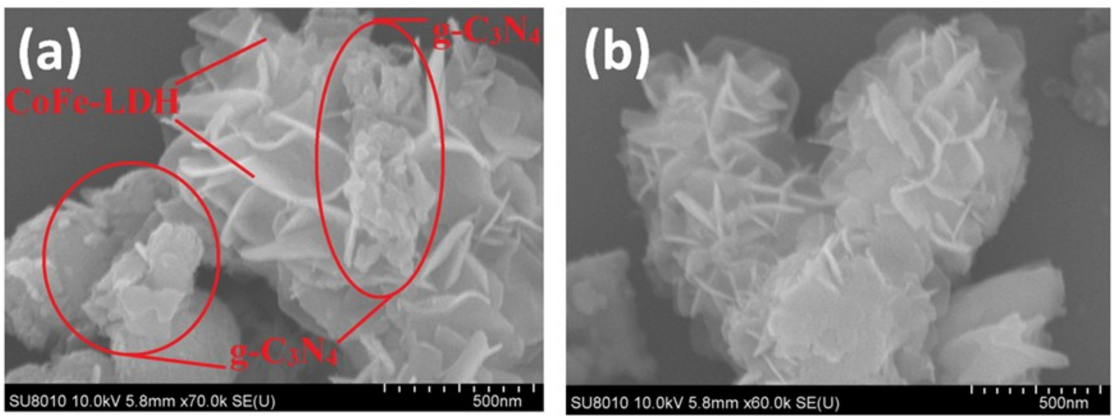


**Figure S11.** SEM images of a physical mixture of CoFe-LDH and g-$C_3N_4$ (a and b)

The scanning electron microscope (SEM) was performed to analyze the morphological and structural features of the physical mixture. SEM images (Figure S11) reveals that individual flower-like CoFe-LDH and g-$C_3N_4$ nanosheets are found. SEM images disclose several separated clumps (poor dispersion) of g-$C_3N_4$ nanosheets on the surface of flower like CoFe-LDH. The low dispersion may enlarge the ion transport distance in the nano-scale dimension, which leads to decrease of the electrochemical active surface area (ECSA) and hence influence the charge transportation for electrochemical water splitting.

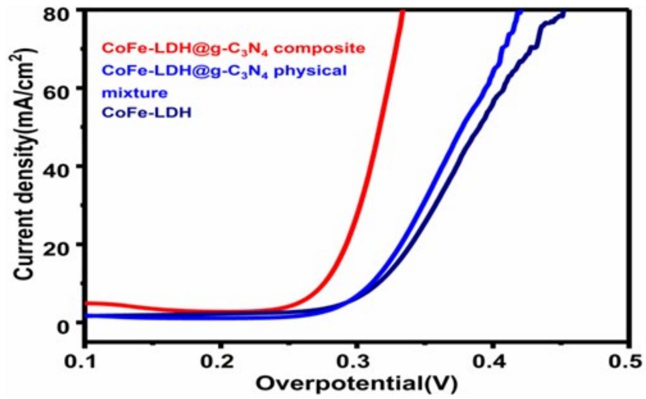


**Figure S12.** (a) Linear scan voltammogram (LSV) OER curves of CoFe-LDH@g-$C_3N_4$ composite and physical mixture of CoFe-LDH and g-$C_3N_4$ nanosheets.

The electrocatalytic activities of CoFe-LDH@g-$C_3N_4$ composites and physical mixture were measured for OER and results indicate the weak catalytic activity of physical mixture (Figure S12).

**Table S1.** Comparison of OER performance for the CoFe-LDH@g-$C_3N_4$ (10%) and recently reported materials

| Catalyst | η(mV @10 mAcm$^{-2}$) | Electrolyte | Substrate | References |
|---|---|---|---|---|
| **CoFe-LDH@g-$C_3N_4$** | **275** | **1M KOH** | **GCE** | **This Work** |
| CoMn-LDH nanosheets | 324 | 1M KOH | GCE | 1 |
| NiCo LDH | 367 | 1.0 M KOH | GCE | 2 |
| $Co_3O_4$/$NiCo_2O_4$ nanocages | 340 | 1.0 M KOH | Ni foam | 3 |
| $CoSe_2$ | 407 | 1 M KOH | CC | 4 |
| MnCoP nanoparticles | 330 | 1 M KOH | GCE | 5 |
| NiFe@g-$C_3N_4$/CNT | 326 | 1 M KOH | GCE | 6 |
| Co4N/CNW/CC | 330 | 1 M KOH | GCE | 7 |
| N-GRW | 360 | 1 M KOH | GCE | 8 |
| Ni-Fe-P | 217 | 1 M KOH | NF | 9 |
| $FeNi_3N$ | 220 | 1 M KOH | NF | 10 |

**Table S2.** Comparison of bifunctional catalyst performance built as two-electrode electrolyzers in 1 M KOH.

| Catalyst | Ej=10 $mAcm^{-2}$ (V) | Electrolyte | Ej=100 $mAcm^{-2}$ (V) | References |
|---|---|---|---|---|
| **CoFe-LDH@g-$C_3N_4$** | **1.55** | **1 M KOH** | **1.80** | **This Work** |
| NiFe LDH | 1.70 | 1M KOH | / | 11 |
| NiSe NWs | 1.63 | 1.0 M KOH | / | 12 |
| NiFe/NF | 1.64 | 1.0 M KOH | / | 13 |
| $Ni_2P$ | 1.63 | 1 M KOH | / | 14 |
| $Ni_3S_2$ | 1.76 | 1 M KOH | / | 15 |
| $FeNi_3N$ | 1.62 | 1 M KOH | / | 10 |
| Porous NiFe/$NiCo_2O_4$/NF | 1.67 | 1 M KOH | 2.12 | 16 |
| NiFeOx/CFP | 1.51 | 1 M KOH | 1.80 | 17 |
| Ni-Fe-P | 1.64 | 1 M KOH | / | 9 |
| Ni-Fe-P@C | 1.52 | 1 M KOH | / | 9 |

## Notes and references


1. F. Song and X. Hu, *J. Am. Chem. Soc.*, 2014, **136**, 16481-16484.
2. H. Liang, F. Meng, M. Cabán-Acevedo, L. Li, A. Forticaux, L. Xiu, Z. Wang and S. Jin, *Nano Lett.*, 2015, **15**, 1421-1427.
3. H. Hu, B. Guan, B. Xia and X. W. Lou, *J. Am. Chem. Soc.*, 2015, **137**, 5590-5595.
4. P. Chen, K. Xu, S. Tao, T. Zhou, Y. Tong, H. Ding, L. Zhang, W. Chu, C. Wu and Y. Xie, *Adv. Mater.*, 2016, **28**, 7527-7532.
5. D. Li, H. Baydoun, C. N. Verani and S. L. Brock, *J. Am. Chem. Soc.*, 2016, **138**, 4006-4009.
6. D. Liu, S. Ding, C. Wu, W. Gan, C. Wang, D. Cao, Z. u. Rehman, Y. Sang, S. Chen, X. Zheng, Y. Wang, B. Ge and L. Song, *J. Mater. Chem. A*, 2018, **6**, 6840-6846.
7. F. Meng, H. Zhong, D. Bao, J. Yan and X. Zhang, *J. Am. Chem. Soc.*, 2016, **138**, 10226-10231.
8. H. B. Yang, J. Miao, S. F. Hung, J. Chen, H. B. Tao, X. Wang, L. Zhang, R. Chen, J. Gao, H. M. Chen, L. Dai and B. Liu, *Sci. Adv.*, 2016, **2**, 1501122.
9. S. H. Ahn and A. Manthiram, *J. Mater. Chem. A*, 2017, 5, 2496-2503.
10. B. Zhang, C. Xiao, S. Xie, J. Liang, X. Chen and Y. Tang, *Chem. of Mate.*, 2016, **28**, 6934-6941.
11. J. Luo, J.-H. Im, M. T. Mayer, M. Schreier, M. K. Nazeeruddin, N.-G. Park, S. D. Tilley, H. J. Fan and M. Grätzel, *Science*, 2014, **345**, 1593-1596.
12. C. Tang, N. Cheng, Z. Pu, W. Xing and X. Sun, *Angew. Chem.*, 2015, 54, 9351-9355.
13. Q. Luo, M. Peng, X. Sun, Y. Luo and A. M. Asiri, *Inter. J.Hyd. Energy*, 2016, **41**, 8785-8792.
14. L.-A. Stern, L. Feng, F. Song and X. Hu, *Energy Environ. Sci.*, 2015, **8**, 2347-2351.
15. L.-L. Feng, G. Yu, Y. Wu, G.-D. Li, H. Li, Y. Sun, T. Asefa, W. Chen and X. Zou, J. Am. *Chem. Soc.*, 2015, **137**, 14023-14026.
16. C. Xiao, Y. Li, X. Lu and C. Zhao, *Adv. Funct. Mater.*, 2016, **26**, 3515-3523.
17. H. Wang, H.-W. Lee, Y. Deng, Z. Lu, P.-C. Hsu, Y. Liu, D. Lin and Y. Cui, *Nat. comm.*, 2015, **6**, 7261.